BULLETIN OF THE POLISH ACADEMY OF SCIENCES
TECHNICAL SCIENCES, Vol. 69(6), 2021, Article number: e139007
DOI: 10.24425/bpasts.2021.139007

FLHex: a flapped-paddle hexapod for all-terrain amphibious locomotion

Piotr BURZYNSKI[2*], Ashutosh SIMHA[1], Ülle KOTTA[1], Ewa PAWLUSZEWICZ[2], and Shivakumar SASTRY[3]

[1] School of Information Technologies, Department of Software Science, Tallinn University of Technology, 12618 Tallinn, Estonia
[2] Bialystok University of Technology, Department of Robotics and Mechatronics, ul. Wiejska 45C, 15-351 Bialystok, Poland
[3] University of Akron, Department of Electrical and Computer Engineering, Akron, Ohio 44325, USA

Abstract. This paper presents the design of a versatile mechanism that can enable new directions in amphibious, all-terrain locomotion. The simple, passive, flapped-paddle can be integrated with several structures that are well-suited for locomotion in terrestrial applications. The flapped-paddle overcomes a serious limitation of the conventional flipper where the net lateral forces generated during oscillatory motion in aquatic environments averages out to zero. The flapped-paddle and its mounting, collectively, rests in natural positions in the aquatic environment so as to maximize hydrodynamic force utilization and consequently the propulsive efficiency. The simplicity of the design enabled us to develop a simulation model that concurs well with experimental results. The results reported in the paper are based on integrating the flapped-paddle with the curved leg of the RHex hexapod robot.

Key words: biologically-inspired robots; amphibious robotics; mechanism design.

1. INTRODUCTION

Asymmetry in design can significantly enhance the propulsive efficiency and versatility in a variety of multi-regime amphibious robotic systems. Robotic systems have been deployed in several critical applications in complex environments, such as disaster management, reconnaissance, mining, and exploration in recent years. Many of these system rely on interesting structures and mechanisms for locomotion in amphibious environments. For example, [1–10] present a few novel bio-inspired ideas for locomotion. Other novel mechanisms that are based on rotation to achieve terrestrial and aquatic locomotion are reported in [11, 12]. An interesting class of amphibious robots, closely related to the one proposed in this paper, is based on the well-known biologically inspired terrestrial robot RHex [13, 14], a hexapod with rotating curved, flexible legs, that allow it to operate in undulatory terrain and inaccessible environments.

The design of structures and mechanisms that are reported in the literature must, however, be adapted for use in terrestrial or aquatic environments. For example, an early amphibious evolution of the RHex platform was the RHex-Aqua [15, 16]. The semicircular legs of the RHex were replaced by a set of flippers that allowed the robot to swim and dive underwater. However, this required manual intervention to replace the flippers. An improved version, AmphiHex, was proposed with a curved leg that could transform into the flipper using a multi-linked, fully actuated mechanism [17–19]. While this mechanism alleviated the need for manual intervention to transition between terrestrial and aquatic environments, such intricate mechanisms perforce require the expenditure of additional energy to adapt to different environments and may introduce additional failure points.

Any mechanism for locomotion must generate forces that can suitably propel the system in multiple regimes. Given the extensive applications for such systems, it is interesting to understand whether there are implicit or explicit design constraints that impede the utilization of these forces and, thus, reduce the propulsive efficiency that can be achieved. The mechanisms must be simple to operate, maximize force utilization in different environments, must not require complex control strategies, and minimize the dependence on expensive sensing and perception capabilities.

In this paper, a novel structure and mechanism for amphibious locomotion that is simple and versatile is presented. It is demonstrated that the propulsive efficiency in a conventional flipper is diminished because of its symmetric structure. In order to effectively move in aquatic media, the lateral drag force, F_y, which is significantly greater than the longitudinal force, F_x, needs to be completely utilized for propulsion i.e., the drag force must not average out to zero. The simulation and experimental results in this paper demonstrate that when a conventional flipper is used in aquatic environments, the drag force averages out to zero and, thus, even when the lateral force generated is larger than the longitudinal force, its utilization for propulsion cannot be achieved. To address this challenge, a simple, passive, flapped-paddle mechanism is proposed that introduces asymmetry in the lateral force by design. The asymmetry in the flapped-paddle structure ensures that the drag force does not average out to zero during the oscillation cycle, thereby enabling effective utilization of the generated forces for locomotion. Further, the flapped-paddle can be easily integrated into a variety of structures to enable

*e-mail: p.burzynski@doktoraci.pb.edu.pl

Manuscript submitted 2021-03-30, revised 2021-07-05, initially accepted for publication 2021-07-28, published in December 2021

amphibious locomotion; the results reported in this paper are based on integrating a flapped-paddle with the curved leg of the RHex. This novel design offers a new mechanism for amphibious locomotion that is:

- **simple** – does not require complex actuation mechanisms for transitioning across terrestrial and aquatic environments,
- **efficient** – completely utilizes the dominant drag forces for locomotion,
- **versatile and robust** – enables the robot to traverse in undulatory terrain, steep obstacles, staircases and aquatic environments without the need for complex control strategies or expensive sensing and perception.

The FLHex design shown in Fig. 1, employs the flapped-paddle which was studied in [21] in underwater environments. This design was in fact inspired by the feathers on a bird's wing, which open on the up-stroke and close on the down-stroke, causing asymmetry in drag force [22, 23]. There are other recent reports that are related to the ideas in this paper. Aquatic mechanisms that rely on asymmetric drag forces are reported in [24] the curved leg is equipped with a paddle which allows the robot to swim on the surface of water using circular strokes such that the paddle is above the surface during one half cycle and below in the other half cycle, thereby generating asymmetric drag force. However, this mechanism does not enable underwater swimming as the net drag force sums up to zero in the stroke cycle. In [25, 26] the actuator comprises stiff fins which give way only in one half of the stroke cycle. In [27] a passive rowing joint which is spring loaded is employed to achieve asymmetry by offering less resistance during the recovery stroke. Yet another approach is to employ skewed actuation i.e. a faster power stroke and slow recovery stroke. Some works in this direction are [28–31]. A drawback of this approach however is the need to significantly reduce the duty cycle of the power stroke, resulting in intermittent and sluggish motion.

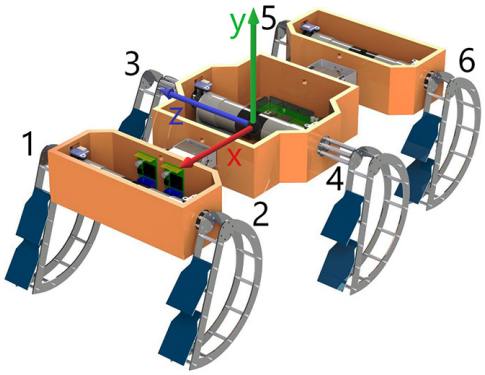

Fig. 1. FLHex: a flapped-paddle hexapod robot (see video in [20])

The paper is organized as follows. Section 2 presents the design of the flapped-paddle and its integration with the curved leg of the RHex hexapod. After presenting the models for locomotion gaits in Section 3, the results from our locomotion trials in Section 4 are presented. Finally, Section 5 presents the conclusions and next steps in this investigation.

2. DESIGN AND FABRICATION

This section describes the flapped-paddle and its integration with the RHex hexapod leg. RHex design specifications are given in Table 1 and Table 2.

Table 1
RHex design specifications

Part	Length [cm]	Height [cm]	Width [cm]	Weight [g]
Leg smaller (×4)	17.4	17.4	3.3	91.2
Leg bigger (×2)	17.4	17.4	8.2	112.4
Mid-module	20	9.5	20	1624
End-module with servos (×2)	9	7	20	1053
total	**55.2**	**21.8**	**36.4**	**3730**

Table 2
RHex design specifications

Part	material
Legs	Acrylic
Body	PLA
Flaps	LDPE

2.1. Flapped-paddle design

The drag and wake forces in aquatic environments primarily comprise the hydrodynamic forces on an oscillating flipper [32–34]. Forces due to lateral displacement of fluid during oscillation, acts perpendicular to the surface of the flipper's to exert the drag force. The wake force is exerted in the longitudinal direction along the surface due to the momentum imparted into the wake behind the fin. In a conventional flipper, the both drag and wake forces are generated, and in fact the lateral drag force significantly dominates the longitudinal wake force in low inflow conditions (see [34]). However, the symmetry in the design of the conventional flipper creates a symmetric lateral drag force during the oscillation cycle; this phenomenon unfortunately causes the average lateral drag force to become zero. Thus propulsion of a robot that uses the conventional flipper, must rely only the wake force. Therefore, the generated forces in a conventional flipper are under-utilized and hence there is a significant decrease in propulsive efficiency. It is important to note that the wake force is significant only when the fin oscillates in a high-inflow velocity regime as explained in [32]. Moreover, it is known that oscillatory motion is unsuitable for turbulent regimes [35]. This is due to the fact that the momentum that is shed off into the wake behind the trailing edge of the flipper, and the resulting force, are linear in the inflow velocity, and therefore are weak in low inflow regimes.

In several underwater robots, it can be seen that lateral drag forces have a much higher magnitude compared to longitudinal forces, though producing zero net thrust. This can be seen for instance in the RHex-Aqua (see Fig. 8 in [16], Fig. 7 in [36]), as well as in our experiments as shown in Fig. 2 which presents

the force exerted on a conventional flipper when placed in an underwater testbed. In Fig. 2, F_y is the lateral drag-force and F_x is the longitudinal force which consists of drag and wake forces, which can be seen to be significantly weaker.

This drawback of conventional flippers is alleviated by the flapped paddle-fin shown in Fig. 3 which comprises a set of flaps mounted in an overlapping louver-like structure, which open during one half-cycle of oscillation i.e., the recovery stroke, and close in the other half i.e. the power stroke. This almost completely asymmetrizes the significantly higher lateral drag-force (as shown in Fig. 2) which can be now be utilized for underwater locomotion, instead of the weaker longitudinal forces. The flapped-paddle mechanism simultaneously increases propulsive efficiency and net thrust, over conventional flippers (see Fig. 7 and Fig. 8 in [21]).

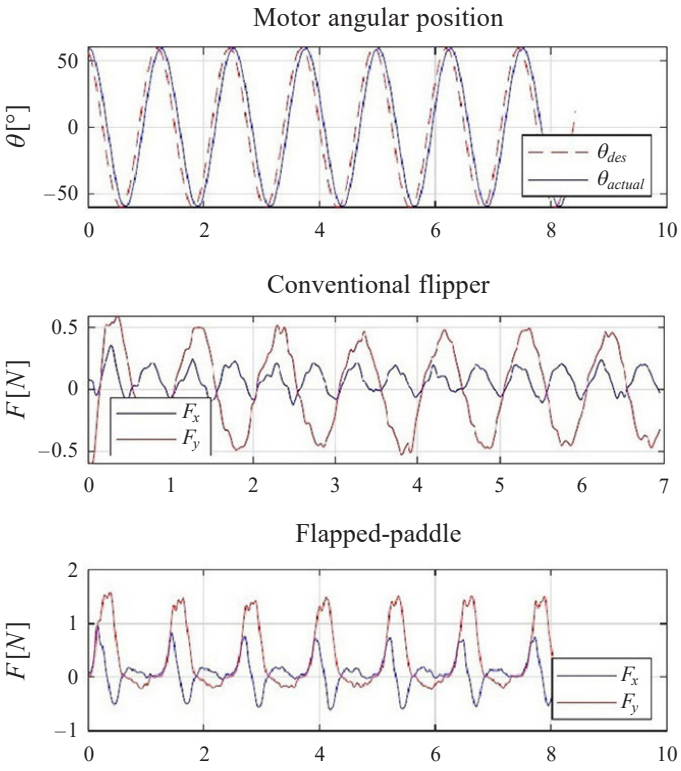

Fig. 2. Asymmetry improves propulsive efficiency. The symmetry in the lateral drag force (F_y) for the conventional flipper (top) results in zero average force in an aquatic environment. Notice that the lateral drag force for the flapped-paddle is suppressed in the recovery stroke, thus maximizing propulsive efficiency because $F_x < F_y$

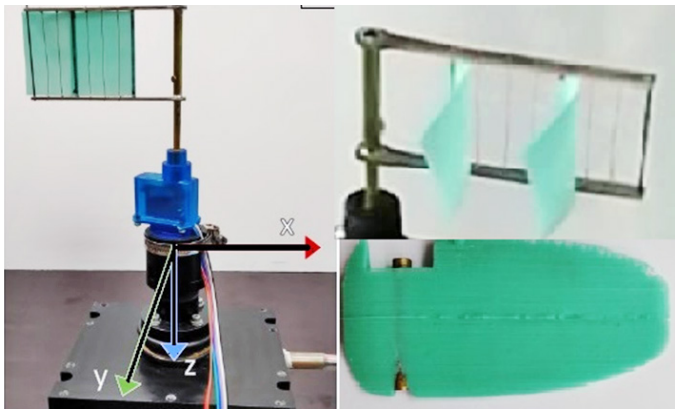

Fig. 3. Flipper mount (left) and structure (right). The symmetry in the structure of the conventional flipper (right, bottom) cancels the lateral drag force; the flapped-paddle (right, above) opens fully in the recovery-stroke and closes in the power stroke; there is little impact on mounting on the test-plate (left)

2.2. Integrating the flapped-paddle into a leg

The flapped-paddle can be integrated into a variety of leg structure. As an initial step, the flapped-paddle was integrated into the curved leg structure of RHex. This results in a semi-circular structure with movable flaps as shown in Fig. 4. The flat portion has a ladder like structure that mounts a set of overlapping flaps. The flaps have very low inertia so as to minimize the delay in opening and closing. The flap-mounting is reinforced with adhesive vinyl in order to maintain some minimal stiffness that ensures that the flaps are constrained from folding over during the recovery stroke. Alternatively, this can also be achieved by constraining using a thin rod or string at the hinge. The operation of the flapped paddle-leg during an oscillatory cycle underwater is illustrated in Fig. 5. We also invite the reader to view the video in [20]). Notice that the flaps open completely during the recovery stroke, early in the cycle. They are then maintained parallel to the flow thereafter and, hence, offering low structural resistance to flow. During the power-stroke they align to form a flat paddle. This mechanism therefore enables a high net drag force which can be effectively used for underwater locomotion. This force is realized because of the design is asymmetrical and the net forces do not average out to zero. By changing the mean angle of oscillation, the net force vector can be redirected to generate appropriate pitch, roll and yaw moments.

The flapped-paddle does not structurally impede terrain locomotion. Similar to [13], the curved portion of the leg allows the robot to traverse highly uneven terrain, including steep obstacles, climb stairs etc.

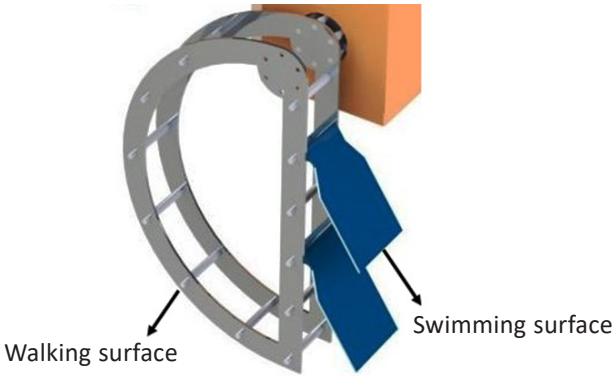

Fig. 4. Multi-regime, composite Fin-Leg. The flapped-paddle can be easily integrated into a variety of mechanical structures to enable both terrestrial and aquatic locomotion. In the above figure, the flapped-paddle has been integrated into the RHex Leg [13]

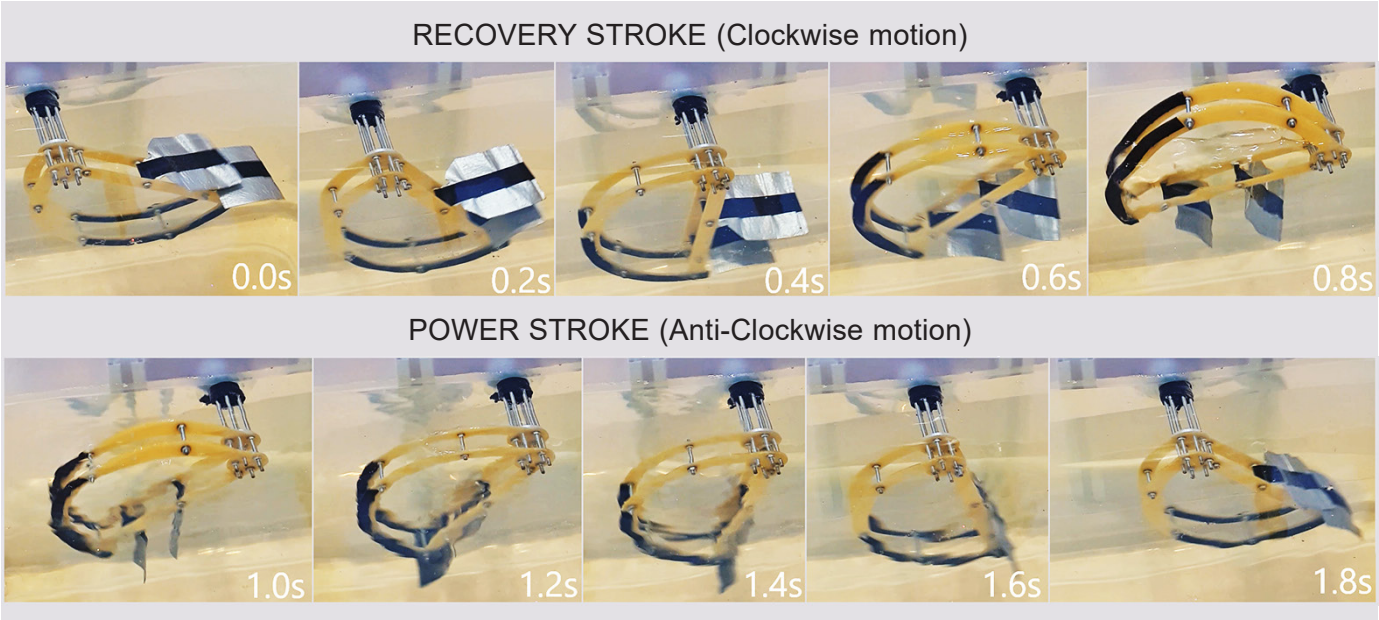

Fig. 5. Responsive design. Note that in aquatic environments the flaps rapidly close to increase the utilization of the power stroke cycle (top). In the recovery stroke, the flaps rest along the structure of the flow, minimizing drag (bottom)

2.3. Robot integration

The FLHex comprises three modules, each with two symmetrically mounted legs that were integrated with flapped-paddles. The joints connecting the modules were driven using servo motors. The legs were controlled using high-torque brushed DC motors with encoders and actuated using a microcontroller. The servo motors connecting the modules were actuated via a PID controller whose gains and set-points were tuned to operate in various terrains, without the need for explicit sensing or perception as demonstrated in the experimental video. Collectively, these steps enabled versatile and robust locomotion. The materials used for the robot are summarized as follows. The body of the robot was made from polylactic acid (PLA), and the legs frames were made from acrylic sheet. The legs were coated with an adhesive foam to prevent slippage during climbing gaits. The flaps were made from Nylon laminated with low-density polyethylene (LDPE). The material for the flaps was chosen such that there is minimal resistance to flow during the recovery stroke and fast opening, as well as minimal bending during the power stroke, to maximize drag-forces.

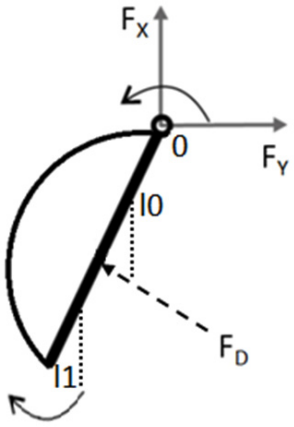

Fig. 6. Force diagram. Drag-forces generated during oscillation in an aquatic environment under low inflow conditions. Note that the flaps rotate in opposite orientation to the leg rotation

3. MODELING LOCOMOTION GAITS

3.1. Propulsive force during swimming

The drag-force generated by the leg during the power stroke of oscillation is given as follows (see [32]).

$$F(t) = \int_{l_0}^{l_1} \frac{1}{2} C_d \rho w \dot{\theta}^2(t) s^2 ds, \tag{1}$$

where l_1 is the length of the leg and l_0 is the distance from the hinge from where the flaps are mounted, C_d is the drag coefficient, w is the width of the flap area, ρ is the fluid density and $\dot{\theta}(t)$ is the angular velocity of oscillation (Fig. 6). The instantaneous drag-force $F(t)$ acts perpendicular to the surface, in a direction opposing the rotation. The convention used here is that the power-stroke and recovery-stroke correspond to decreasing and increasing θ respectively. During the recovery-stroke one assumes a reduced width of the surface element obstructing the flow, i.e., $w_r \ll w$, and change the direction of the (negligible) drag force as

$$F(t) = -\int_{l_0}^{l_1} \frac{1}{2} C_d \rho w_r \dot{\theta}^2(t) s^2 ds. \tag{2}$$

The components of hydrodynamic forces on the force plate under zero inflow condition are obtained as follows.

$$F_x(t) = F_D(t)\sin\big(\theta(t)\big),$$
$$F_y(t) = F_D(t)\cos\big(\theta(t)\big). \tag{3}$$

A comparison between forces generated using the above model, and forces measured by the testbed when oscillating the flapped-paddle is shown in Fig. 7.

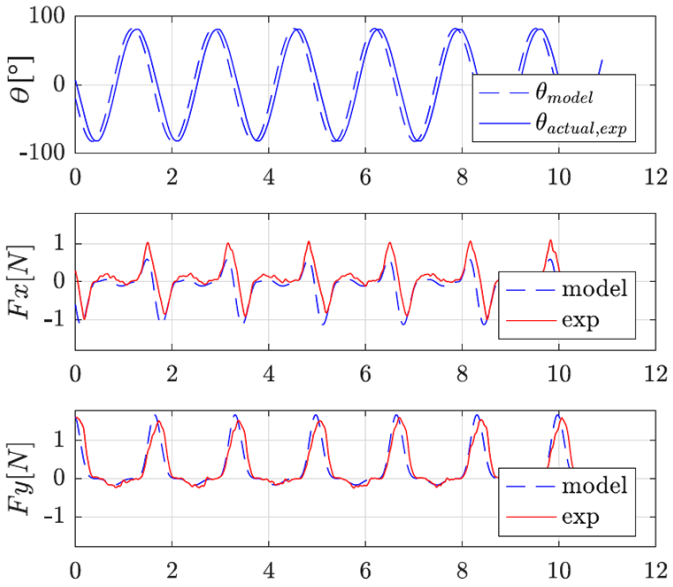

Fig. 7. Ease of design. The simplicity of the flapped-paddle and the low impact of the hydrodynamic artifacts, enabled us create high-fidelity models. The above figure shows the lateral and longitudinal forces, with $l_0 = 3$ cm, $l_1 = 10$ cm, $w = 6$ cm, $w_r = 0.6$ cm, obtained using models (Eq. (3)) and experiments

The swimming gait, i.e., angular position $\theta(t)$ of the DC motor, is chosen as the following sinusoidal wave with offset

$$r(t) = \frac{A}{2}\sin(2\pi f t) + A_0. \tag{4}$$

This reference is tracked by the DC motor driving the leg, using a PID control law. Here, the offset A_0 is used to steer the mean force vector, which can be used for achieving different swimming gaits.

3.2. Terrestrial gait design

For locomotion on flat ground, the motors corresponding to legs 1, 4, 5 (i.e., set A) and legs 2, 3, 6 (i.e., set B) as indicated in Fig. 1, are respectively synchronized, and alternatively actuated such that when set A is in contact with the ground (i.e., *contact gait*) while set B has lifted off (i.e., *recovery gait*). The gait during one time-period is designed as follows. The contact gait is designed as

$$\theta_r(t) = -\alpha + \frac{4\alpha t}{T}, \quad \forall t \in [0,\, T/2), \tag{5}$$

and the recovery gait as

$$\theta_r(t) = \alpha + \frac{4(\pi - \alpha)(t - T/2)}{T}, \quad \forall t \in [T/2,\, T), \tag{6}$$

where α is the stride angle and T is the time period of the entire gait. The idea behind this simple gait is that when one set of legs complete their contact stride and are about to lift off, the other set come in contact with the ground. This ensures that the robot is supported by at least 3 legs at any given time, within a contact angle of α.

The time period T is decided based on the RPM limitations of the motor, while the stride α is decided by the torque saturation limits of the motor (heuristically) as $^m/_3\, L \sin\alpha < \tau$, where τ is the limiting torque, L is the length of the leg and m is the mass of the robot. The assumption made here is that the inertia of the leg is comparatively negligible and the mass is equally shared between the legs.

The above reference gait motor command is tracked using a nonlinear PID control law on the unit circle $\mathbb{S}^1$, for the motor torque as

$$U = k_p \sin(\theta - \theta_r) + k_d\dot{\theta} + k_i \int_0^t \sin(\theta - \theta_r)d\theta, \tag{7}$$

where k_p, k_d, k_i are control gains.

The locomotion gait reference and the closed loop tracking performance for flat surface is indicated in Fig. 8.

For undulatory surfaces, the reference gait is not modified, and this includes the case of steep obstacles as well. Here, the undulations are considered as disturbance torques, and are compensated by the integral component.

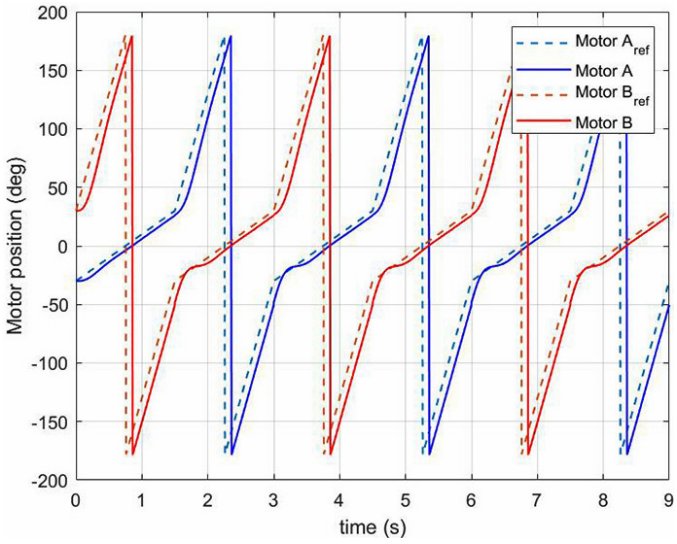

Fig. 8. Terrestrial gait (Buehler clock [13]). Motor reference command and tracking for terrestrial locomotion, with $\alpha = 30°$, $T = 3\,s$

3.3. Controller implementation

A Polulu motor (37Dx70L) with 50:1 gearbox and quadrature encoder that provided 3200 signals per turn was used. The motor was driven by a VNH5019 controller. Every leg of the robot was independently controlled by such a motor-controller pair.

The main strategy used in the implementation was to control the position of each leg independently. This avoided the need to explicitly synchronize their position reference trajectories, which is nontrivial especially when each leg encounters an undulating terrain. Since the relevant part of the control is only when the leg is in contact with the ground, a higher sampling rate was used to capture the motor encoder values and the tracking error and hence know the error from the desired position; this also compensates for external noise. In each iteration of the PID loop, all the error variables were computed. The updated controller signal (PWM duty cycle) was computed in accordance with the sampling rate associated with the position of the leg. The sampling was also allows to be non-uniform, which allowed more accurate motor control when the leg is in contact, where the noisy forces are higher, than when the leg is rotating freely. The use of an optical encoder allowed us to determine the absolute position, circumventing the need to design velocity controllers which indirectly control the motor position.

4. LOCOMOTION TRIALS

Locomotion trials with the FLHex were performed in different environments. We invite the reader to view the **attached video** [20] where the experiments were recorded.

4.1. Terrestrial trials

Snapshots of walking on a flat surface as well as over obstacles using the walking gait in Fig. 8, are presented in Fig. 9. This demonstrates that the platform is robust to terrain undulations and steep obstacles, as the walking gait need not be explicitly adapted to terrain variations. This robustness mitigates the dependence on additional sensors for profiling the terrain undulation and varying the reference command. Moreover, the modular structure also adds to the robustness as the servo control law allows the modules to reconfigure their joint angles so as to additionally compensate for disturbance loads due to undulations.

In Fig. 10 the staircase climbing gait is demonstrated. Here, the reference gait is modified as a constant angular velocity, in-phase rotation of the front and rear pair of legs, while the middle pair is deactivated. The reason for this is that without the middle pair, the gait is robust to varying profiles of staircases, while activating the middle pair requires additional sensing for avoiding overturning of the robot. During this gait, the reference position of the modular joint angles is varied such that the front and rear modules are lifted up, so as to minimize the load on the DC motors. From the video, it can also be noticed that the control law is saturated such that the gait of a particular leg is temporarily paused when the load is higher, and resumes only when this is relieved due to other legs coming in contact with the stairs. During the climbing gaits, the servo motors

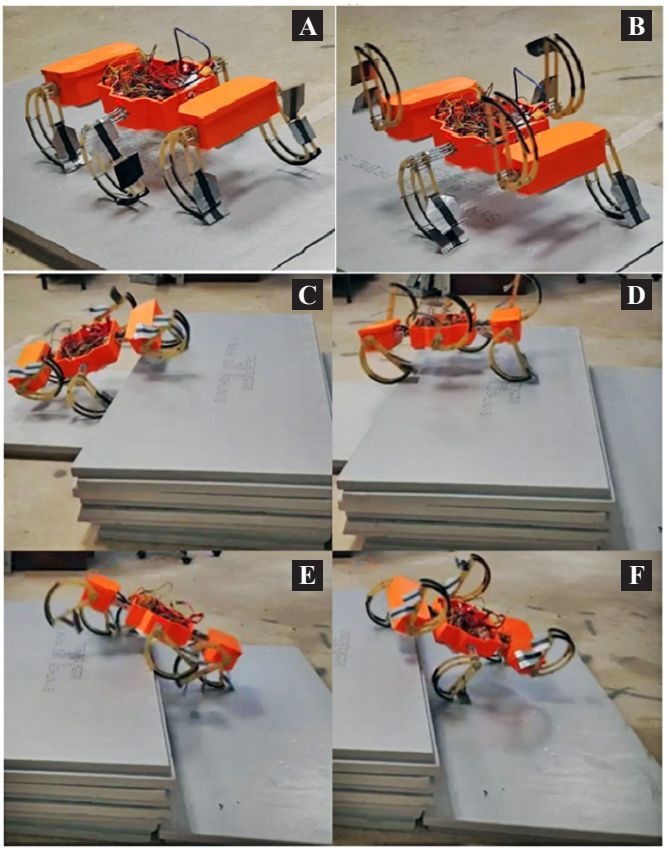

Fig. 9. Versatility of terrestrial gait. FLHex easily adapts to terrain changes without the need for explicitly changing the gait, which may require sensing or perception

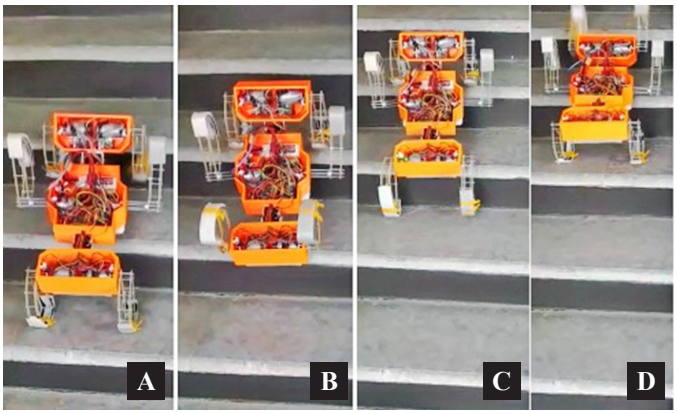

Fig. 10. Staircase climbing. FLHex can traverse stairways when the motion of the front and rear legs are synchronized

controlling the modular-joint angles were modulated such that the front and rear modules were oriented upwards. This enables a higher degree of stability when climbing, and also increasing the possible step size.

Table 3 summarizes the effect of varying the stride angle α and time period T in the walking gait defined above in Eq. (6). Note that here x is the total displacement, and y is the displacement/cycle. For each pair of (α, T) the robot was made to walk

Table 3
RHex design specfications

	$T = 2s$	$T = 1s$	$T = 0.75s$
$\alpha = 20°$	x = 145 cm y = 29 cm	x = 295 cm y = 29.5 cm	x = 342 cm y = 25.65 cm
$\alpha = 30°$	x = 209 cm y = 41.8 cm	x = 374 cm y = 37.4 cm	x = 483 cm y = 36.23 cm
$\alpha = 40°$	x = 263 cm y = 52.6 cm	x = 545 cm y = 54.5 cm	x = 628 cm y = 47.1 cm
$\alpha = 45°$	x = 287 cm y = 57.4 cm	x = 532 cm y = 53.2 cm	x = 644 cm y = 48.3 cm

for 10s, and the average value obtained over 5 trials has been computed. The total number of trials overall was therefore 60. It can be seen that the total displacement (and consequently average speed) increased with increasing α and decreasing T. The maximal displacement/cycle $y = 57.4$ cm was observed when $\alpha = 45°$ and $T = 2s$, indicating a larger stride angle and smaller rotational velocity may be optimal. Often due to motor limitations, there is a need to trade off between using a large stride angle (in case the motor has a larger torque rating) or smaller rotation time period (in case the motor has a higher RPM rating). In this case, the above table would help designers in selecting an appropriate driving motor for the legs.

The video link [20] also includes experiments where the robot transitions from swimming onto land, to demonstrate its amphibious capability. Due to the limitations of fabrication facilities, the current version of the robot is not water-proof and therefore needed a supporting flotation appendage. However future extensions have been planned to incorporate a completely water-proof version.

4.2. Swimming trials

Snapshots of surface swimming with a gait as shown in Fig. 7 are presented in Fig. 11. Here it can be seen that the flaps open up during the recovery-stroke and close during the power-stroke. All 6 legs are synchronized in this gait. As visible from the attached video [20], turning maneuvers can be performed by actuating only one side (or minimally actuating the other side).

Note that the current platform has not been water-proofed which is why the diving gaits have not been experimentally characterized. The robot was mounted on a floating platform in order to perform aquatic trials. This platform introduced additional rotational and translational drag forces when swimming.

Table 4 summarizes the effect of varying the frequency f and amplitude A of the swimming gait Eq. (40). Note that here x is the total displacement, and y is the displacement/cycle. For each pair of (f, A) the robot was made to swim for 10s, and the average value obtained over 5 trials has been computed. The total number of trials overall was therefore 45. It can be seen that the total displacement (and consequently average speed) increased with increasing f and A. The maximal displacement/cycle $y = 39$ cm was observed when $A = 160°$ and $f = 0.5$ Hz. The above table indicates that maximizing the stroke amplitude at the cost of a lower stroke frequency may be optimal (in terms of maximizing displacement/cycle).

Table 4
Parametric study of swimming gait

	$f = 0.5$ Hz	f = 1 Hz	$f = 1.33$ Hz
$A = 80°$	x = 95 cm y = 19 cm	x = 150 cm y = 15 cm	x = 210 cm y = 15.75 cm
$A = 120°$	x = 155 cm y = 31 cm	x = 223 cm y = 22.3 cm	x = 270 cm y = 20.25 cm
$A = 160°$	x = 195 cm y = 39 cm	x = 360 cm y = 36 cm	x = 480 cm y = 36 cm

5. DISCUSSION

The primary purpose of this paper was to demonstrate that the popular RHex platform could be easily extended to an amphibious robot, with minimal design modifications. The

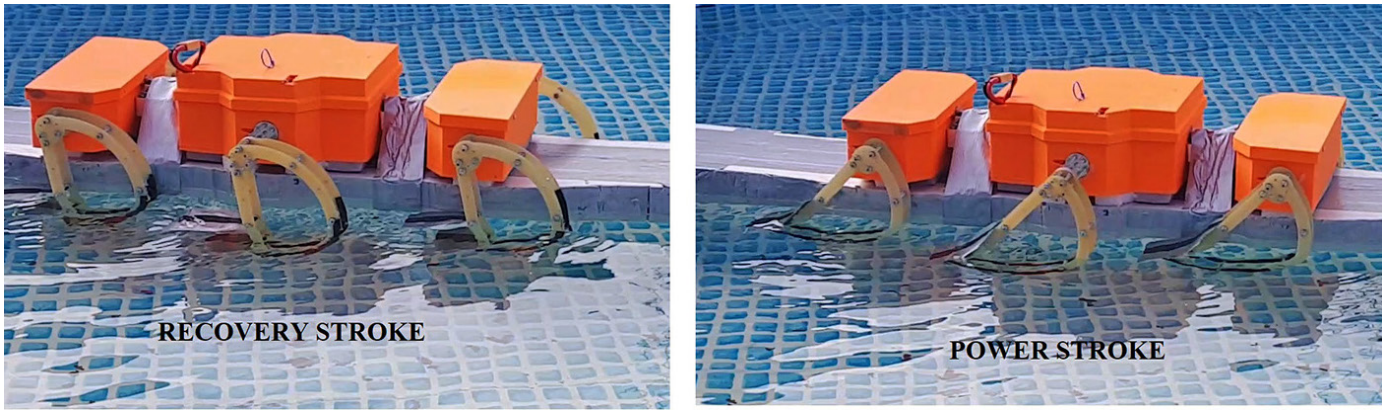

Fig. 11. Amphibious locomotion. The above figure shows the experimental setup for FLHex in water-surface test with $A = 50°$, $A_0 = 20°$, $f = 0.5$ Hz (Eq. (4))

versatility of the flapped-paddle mechanism allowed us to easily integrate it into the RHex leg. In [21], it was shown that the flapped-paddle fin robot was capable of agile underwater and surface swimming gaits. Since the FLHex is also based on the asymmetric flapped paddle, one can easily extrapolate from the experimental results in this paper that FLHex, along with its demonstrated terrestrial gaits and surface swimming capability, is also capable of underwater gaits similar to [21]. Moreover, in Section 3 it was shown that the asymmetric drag based aquatic gait can be easily modeled with appreciable accuracy, rendering FLHex well-suited for model-based control and guidance. The original RHex design included legs which were compliant, as the 'C'-shaped legs were compressible. However, the flat section which mounts the flaps, now prevents the legs from being compressed on impact. In order to include the compressive/shock-absorbing effect of the original RHex leg, the current design includes a foam padding at the bottom of the legs, which in addition to providing resistance to slippage, also provides a shock absorbing effect which is useful for undulatory terrain.

6. CONCLUSIONS

This paper presented the design for a novel flapped-paddle mechanism for enabling amphibious locomotion. This flapped-paddle was integrated with the curved leg of the RHex hexapod to investigate its behavior in terrestrial and aquatic environments. The design is simple and versatile. In addition, the mechanism can be easily integrated into a variety of structures to suit application demands for locomotion.

The results demonstrated that FLHex, our hexapod integrated with the flapped-paddle, is versatile and can traverse undulatory terrains without the need for complex control strategies or expensive sensing and perception. In addition, it seamlessly transitions between aquatic and terrestrial environments by using a simple oscillatory gait, without the need to replace the leg with flippers, or reconfigure the leg. Experimental results in a low-inflow aquatic regime demonstrated that the flapped-paddle offers a significant advantage over conventional flippers by harnessing the dominant drag force. At the core, this design demonstrated that asymmetry in design can significantly enhance the propulsive efficiency and versatility in a variety of multi-regime amphibious robotic systems.

In the future, this systems can be made more robust and waterproof to investigate the performance of the flapped-paddle in more complex aquatic maneuvers including diving and surfacing. Further extensions related to this mechanism can include new control theoretic approaches for locomotion and fault tolerance.

ACKNOWLEDGEMENTS

- The authors thank the labs and engineers at Bialystok University of Technology, Poland and Tallinn University of Technology, Estonia for providing testing and instrumentation facilities.
- P. Burzynski and A. Simha are joint first authors. The work of Piotr Burzynski was supported by the Bialystok Technical University grant No. WI-WM-IIM/7/2020. The work of Ewa Pawluszewicz was supported by the Bialystok Technical University grant No. WZ/WM-IIM/1/2019. The work of Ü. Kotta was supported in part by the Estonian Centre of Exellence in IT, funded by the European Regional Development Fund.

REFERENCES

[1] A. Crespi, K. Karakasiliotis, A. Guignard, and A.J. Ijspeert, "Salamandra robotica II: an amphibious robot to study salamander-like swimming and walking gaits," *IEEE Trans. Rob.*, vol. 29, no. 2, pp. 308–320, 2013.

[2] M. Gad-El-Hak, "Coherent structures and flow control: genesis and prospect," *Bull. Pol. Acad. Sci. Tech. Sci.*, vol. 67, no. 3, pp. 411–444, 2019.

[3] A.J. Ijspeert, A. Crespi, D. Ryczko, and J.M. Cabelguen, "From swimming to walking with a salamander robot driven by a spinal cord model," *Science*, vol. 315, no. 5817, pp. 1416–1420, 2007.

[4] E. Natarajan, K.Y. Chia, A.A.M. Faudzi, W.H. Lim, Ch.K. Ang, and A. Jafaari, "Bio Inspired Salamander Robot with PneuNet Soft actuators-Design and Walking Gait Analysis," *Bull. Pol. Acad. Sci. Tech. Sci.*, vol. 69, no. 3, 2021, Article number: e137055, doi: 10.24425/bpasts.2021.137055.

[5] K. Karakasiliotis and A.J. Ijspeert, "Analysis of the terrestrial locomotion of a salamander robot," *Proceedings of the IEEE/RSJ International Conference on Intelligent Robots and Systems*, St. Louis 2009, pp. 5015–5020.

[6] P. Liljebäck, Ø. Stavdahl, K.Y. Pettersen, and J.T. Gravdahl, "Mamba-A waterproof snake robot with tactile sensing," in *Proceedings of the 2014 IEEE/RSJ International Conference on Intelligent Robots and Systems*, Chicago, IL, US, 2014, pp. 294–301.

[7] S. Hirose and H. Yamada, "Snake-like robots machine design of biologically inspired robots," *IEEE Rob. Autom. Mag.*, vol. 3, 2009.

[8] J. Yu, R. Ding, Q. Yang, M. Tan, and J. Zhang, "Amphibious Pattern Design of a Robotic Fish with Wheel-propeller-fin Mechanisms," *J. Field Rob.*, vol. 30, no. 5, pp. 702–716, 2013.

[9] J. Yu, R. Ding, Q. Yang, M. Tan, W. Wang, and J. Zhang, "On a bio-inspired amphibious robot capable of multimodal motion," *IEEE/ASME Trans. Mechatron.*, vol. 17, no. 5, pp. 847–856, 2011.

[10] T. Paschal, M.A. Bell, J. Sperry, S. Sieniewicz, R.J. Wood, and J.C. Weaver, "Design, fabrication, and characterization of an untethered amphibious sea urchin-inspired robot," *IEEE Rob. Autom. Lett.*, vol. 4, no. 4, pp. 3348–3354, 2019.

[11] V. Kaznov and M. Seeman, "Outdoor navigation with a spherical amphibious robot," *Proceedings of the IEEE/RSJ International Conference on Intelligent Robots and Systems*, Taipei, Taiwan 2010, pp. 5113–5118.

[12] Y. Shen, Y. Sun, H. Pu and S. Ma, "Experimental verification of the oscillating paddling gait for an ePaddle-EGM amphibious locomotion mechanism," *IEEE Rob. Autom. Lett.*, vol. 2, no. 4, pp. 2322–2327, 2017.

[13] U. Saranli, M. Buehler, and D.E. Koditschek, "Design, modeling and preliminary control of a compliant hexapod robot," in *Proceedings of the 2000 IEEE International Conference on Robotics and Automation*, San Francisco,CA, 2000, vol.3, pp. 2589–2596.

[14] U. Saranli, M. Buehler, and D.E. Koditschek, "RHex: A simple and highly mobile hexapod robot," *Int. J. Rob. Res.*, vol. 20, no. 7, pp. 616–631, 2001.

[15] G. Dudek *et al*., "Aqua: An amphibious autonomous robot," *Computer*, vol. 40, no. 1, pp. 46–53, 2007.

[16] Ch. Georgiades, M. Nahon, and M. Buehler, "Simulation of an underwater hexapod robot," *Ocean Eng*., vol. 36, no. 1, pp. 39–47, 2009.

[17] X. Liang *et al*., "The amphihex: A novel amphibious robot with transformable leg-flipper composite propulsion mechanism," in *Proceedings of the IEEE/RSJ International Conference on Intelligent Robots and Systems*, Vilamoura, Algarve, Portugal, 2012, pp. 3667–3672.

[18] S. Zhang, X. Liang, L. Xu, and M. Xu, "Initial development of a novel amphibious robot with transformable fin-leg composite propulsion mechanisms," *J. Bionic Eng*., vol. 10, no. 4, pp.434–445, 2013.

[19] S. Zhang, Y. Zhou, M. Xu, X. Liang, J. Liu, and J. Yang, "AmphiHex-I: locomotory performance in amphibious environments with specially designed transformable flipper legs," *IEEE/ASME Trans. Mechatron*., vol. 21, no. 3, p. 1720–1731, 2015.

[20] P. Burzyński, Poland, FLHex: A Flapped-Paddle Hexapod, (Aug. 01, 2021). [Online Video]. Available: https://www.youtube.com/watch?v=Ux1AlOFUUco (Accessed: Aug. 2, 2021).

[21] A. Simha, R. Gkliva, Ü. Kotta, and M. Kruusmaa, "A Flapped Paddle-Fin for Improving Underwater Propulsive Efficiency of Oscillatory Actuation," *IEEE Rob. Autom. Lett*., vol. 5, no. 2, pp. 3176–3181, 2020.

[22] K.E. Crandell and B.W. Tobalske, "Kinematics and aerodynamics of avian upstrokes during slow flight," *J. Exp. Biol*., vol. 218, no. 16, pp. 2518–2527, 2015.

[23] W. Yang and B. Song, "Experimental investigation of aerodynamics of feather-covered flapping wing," *Appl. Bionics Biomech*., vol. 2017, 2017, Article ID: 3019640. doi: 10.1155/2017/3019640.

[24] B.B. Dey, S. Manjanna, and Dudek G., "Ninja legs: Amphibious one degree of freedom robotic legs," in *Proceedings of the 2013 IEEE/RSJ International Conference on Intelligent Robots and Systems*, Tokio, Japan, 2013, pp. 5622–5628.

[25] S.B.A. Kashem, S. Jawed, A. Jubaer, and Q. Uvais, "Design and Implementation of a Quadruped Amphibious Robot Using Duck Feet," *Robotics*, vol. 8, no. 3, p. 77, 2019, doi: 10.3390/robotics8030077.

[26] B. Kwak and J. Bae, "Design of hair-like appendages and comparative analysis on their coordination toward steady and efficient swimming," *Bioinspir. Biomim*., vol. 12, no. 3, p. 036014, 2017, doi: 10.1088/1748-3190/aa6c7a.

[27] S.B. Behbahani and X. Tan, "Design and modeling of flexible passive rowing joint for robotic fish pectoral fins," *IEEE Trans. Rob*., vol. 32, no. 5, pp. 1119–1132, 2016.

[28] Ch.J. Esposito, J.L. Tangorra, B.E. Flammang, and G.V. Lauder, "A robotic fish caudal fin: effects of stiffness and motor program on locomotor performance," *J. Exp. Biol.*}, vol. 215, no. 1, pp. 56–67, 2012.

[29] G.V. Lauder, "Function of the caudal fin during locomotion in fishes: kinematics, flow visualization, and evolutionary patterns," *Am. Zool*., vol. 40, no. 1, pp. 101–122, 2000.

[30] S.C. Licht, M. Wibawa, F.S. Hover, and M.S. Triantafyllou, "Towards amphibious robots: Asymmetric flapping foil motion underwater produces large thrust efficiently," Technical Raport, Massachusetts Institute of Technology. Sea Grant College Program, 2009.

[31] Ch. Meurer, A. Simha, Ü. Kotta, and M. Kruusmaa, "Nonlinear Orientation Controller for a Compliant Robotic Fish Based on Asymmetric Actuation," in *Proceedings of the International Conference on Robotics and Automation (ICRA)*, Montreal, Canada, 2019, pp. 4688–4694.

[32] G.V. Lauder and E.D. Tytell, "Hydrodynamics of undulatory propulsion," *Fish Physiol*., vol. 23, pp. 425–468, 2005.

[33] M. Bozkurttas, J. Tangorra, G. Lauder, and R. Mittal, "Understanding the hydrodynamics of swimming: From fish fins to flexible propulsors for autonomous underwater vehicles," *Adv. Sci. Technol*., vol.58, pp. 193–202, 2008.

[34] N. Martin, Ch. Roh, S. Idrees, and M. Gharib, "To flap or not to flap: comparison between flapping and clapping propulsions," *J. Fluid Mech*., vol.822, p. R5, 2017, doi: 10.1017/jfm.2017.252.

[35] M. Sfakiotakis, D.M. Lane, and J.B.C. Davies, "Review of fish swimming modes for aquatic locomotion," *IEEE J. Oceanic Eng*., vol. 24, no. 2, pp. 237–252, 1999.

[36] R. Gkliva, M. Sfakiotakis, and M. Kruusmaa, "Development and experimental assessment of a flexible robot fin," in *Proceedings of the 2018 IEEE International Conference on Soft Robotics (RoboSoft)*, Livorno, Italy, 2018, pp. 208–213.